JOURNAL OF CATALYSIS 104, 441–453 (1987)

HCN Synthesis from CH_4, NH_3, and O_2 on Clean Pt*

D. HASENBERG† AND L. D. SCHMIDT

Chemical Engineering and Materials Science, University of Minnesota, Minneapolis, Minnesota 55455

Received August 21, 1986; revised November 1986

Rates of reactions in HCN synthesis were measured between 0.01 and 10 Torr on clean Pt foils between 600 and 1500 K in a steady state flow reactor attached to an analysis system equipped with AES for surface analysis. Addition of O_2 to a 1 : 1 CH_4 : NH_3 mixture at foil temperatures between 1000 and 1400 K caused the HCN production to fall while NO rose to become the dominant product. The CO production rate was lower than that of NO, and very small amounts of CO_2 were formed. AES showed that addition of O_2 produces a reduction of surface carbon from approximately a monolayer to a small coverage. Oxygen appears to react with NH_3 to form NO faster than with CH_4 to form CO. However, NO is capable of reacting with CH_4 to produce HCN so that NH_3 does not oxidize totally to N_2. The rates of CH_4 oxidation and the rate of formation of HCN from CH_4 and NO were also examined. Individual rates are fit to Langmuir–Hinshelwood models, and the rates and selectivities predicted by the rate equations agree well with experiments. These results indicate that under the conditions of industrial HCN synthesis HCN is produced mostly by the NH_3 + CH_4 and CH_4 + NO reactions.

INTRODUCTION

Hydrogen cyanide is prepared industrially by reacting an approximately 1 : 1 : 1 mixture of CH_4, NH_3, and O_2 over a $\frac{1}{4}$-in.-thick layer of Pt–10% Rh gauze at 1400 K with a contact time of several milliseconds (*1*). Yields of 60–70% HCN are obtained, with other major products being N_2, CO, H_2O, H_2, and CO_2. The overall stoichiometric reactions describing HCN synthesis are

$$CH_4 + NH_3 + \tfrac{3}{2}O_2 \rightarrow HCN + 3H_2O \qquad \Delta H^\circ_{298} = -114 \text{ kcal/mole} \quad (1)$$

and

$$CH_4 + NH_3 \rightarrow HCN + 3H_2 \qquad \Delta H^\circ_{298} = +60 \text{ kcal/mole} \quad (2)$$

The second reaction, while having a favorable equilibrium yield above 1000 K, is strongly endothermic, and O_2 must be added to achieve reaction temperatures in an adiabatic gauze reactor. In spite of their industrial importance, these systems have not recently been studied systematically.

We have been studying the surface reactions in the CH_4, NH_3, O_2 system on Pt, Rh, and Pd for several years (*2, 3*). In the absence of O_2, we have found that the process can be described through two major surface reaction steps:

$$CH_4 + NH_3 \rightarrow HCN + 3H_2 \quad (3.1)$$

and

$$NH_3 \rightarrow \tfrac{1}{2}N_2 + \tfrac{3}{2}H_2, \quad (3.2)$$

with results being correlated semiquantitatively over wide ranges of temperature and composition by modified Langmuir–Hinshelwood rate expressions:

$$r_{HCN} = k_{HCN}\theta_c(1 - \theta_c)^n P_{NH_3} = \frac{K_1 P_{CH_4} P_{NH_3}^{1/2}}{(1 + K_2 P_{CH_4}/P_{NH_3}^{1/2})^{n+1}} \quad (4)$$

and

$$r_{N_2} = k_{N_2}(1 - \theta_c)^n P_{NH_3} = \frac{K_3 P_{NH_3}}{(1 + K_2 P_{CH_4}/P_{NH_3}^{1/2})^n} \quad (5)$$

* This work was partially supported by the NSF under Grant DMR82126729.

† Present address: Union Carbide Corporation, South Charleston, West Virginia.

0021-9517/87 $3.00

where θ_c is the coverage of a surface carbon species, n is the number of vacant sites required for NH_3 adsorption, and the K's are groupings of temperature-dependent rate coefficients and equilibrium constants as will be discussed later. The factors $(1 - \theta_c)^n$ arise from an assumption of carbon blocking n surface sites for NH_3 adsorption. These expressions predict the observed strong inhibition of both rates in excess CH_4 with $n = 3$ for Pt and $n = 4$ for Rh.

In this paper we examine the reactions in this system in the presence of O_2. We assume that these may be written as bimolecular and unimolecular reaction steps:

$$CH_4 + NH_3 \rightarrow HCN + 3H_2 \quad (6.1)$$

$$NH_3 \rightarrow \tfrac{1}{2}N_2 + \tfrac{3}{2}H_2 \quad (6.2)$$

$$NH_3 + \tfrac{5}{4}O_2 \rightarrow NO + \tfrac{3}{2}H_2O \quad (6.3)$$

$$NH_3 + \tfrac{3}{4}O_2 \rightarrow \tfrac{1}{2}N_2 + \tfrac{3}{2}H_2O \quad (6.4)$$

$$CH_4 + \tfrac{3}{2}O_2 \rightarrow CO + 2H_2O \quad (6.5)$$

$$CH_4 + 2O_2 \rightarrow CO_2 + 2H_2O \quad (6.6)$$

$$CO + \tfrac{1}{2}O_2 \rightarrow CO_2 \quad (6.7)$$

$$H_2 + \tfrac{1}{2}O_2 \rightarrow H_2O \quad (6.8)$$

$$CH_4 + NO \rightarrow HCN + H_2O + \tfrac{1}{2}H_2 \quad (6.9)$$

$$CH_4 + 4NO \rightarrow CO_2 + 2H_2O + 2N_2 \quad (6.10)$$

$$NH_3 + NO \rightarrow N_2 + H_2O + \tfrac{1}{2}H_2 \quad (6.11)$$

$$NO + H_2 \rightarrow \tfrac{1}{2}N_2 + H_2O \quad (6.12)$$

$$NO + CO \rightarrow \tfrac{1}{2}N_2 + CO_2 \quad (6.13)$$

$$CO + H_2O \rightarrow CO_2 + H_2 \quad (6.14)$$

$$HCN + H_2O \rightarrow NH_3 + CO \quad (6.15)$$

All of these reactions have favorable equilibrium constants (*2*). The decoupling of surface reaction kinetics is arbitrary, but these reaction steps appear to be the dominant ones overall if reactant species shown in the equations are reacted alone over Pt or Rh. In a gas mixture the reactants adsorb and then they or their fragments react on the surface to form products, so that the separation implied by the above steps may still be approximately valid. We shall attempt to test this hypothesis from the experiments described here.

The first two reactions in Eq. (6) are the reactions observed in the absence of O_2, and we assume that Eqs. (6.1) and (6.9) are the only reactions leading to HCN. Equations (6.3)–(6.6) are oxidation reactions of the fuels. Ammonia oxidation (*4–6*) and CH_4 oxidation (*7–9*) have been studied extensively on Pt surfaces, with NO, N_2, CO, H_2O, and CO_2 being the only significant product species observed.

Nitric oxide, an intermediate in NH_3 oxidation, can react with CH_4, NH_3 (*10*), or H_2, Eqs. (6.9)–(6.13), only the first being a route to HCN. The water gas shift reaction, Eq. (6.14), interconnects CO, CO_2, H_2, and H_2O which are products in most reactions. Finally, HCN can be consumed by either hydrolysis, Eq. (6.15), oxidation, or polymerization. These reactions have poorly understood kinetics which we shall assume to be negligible compared to the other reactions.

In this paper we examine the products formed in CH_4, NH_3, and O_2 mixtures and also two bimolecular reactions of two component systems: $CH_4 + O_2$ (Eqs. (6.5) and (6.6)) and CH_4 + NO (Eqs. (6.9) and (6.10)). Our objectives are to determine which reactions produce HCN and to obtain rates of each reaction. The overall goal of these experiments is to determine the surface species that lead to each product and thus find the surface reaction mechanisms.

EXPERIMENTAL

Reaction rates were obtained in a stainless steel reactor (*2, 3*) attached to an ultrahigh vacuum system for analysis of surfaces before and after reaction by Auger electron spectroscopy (AES). Samples were polycrystalline Pt foils of ~1 cm^2 area mounted on plugs with Pt–Rh thermocouples for temperature measurement. Samples were transferred between reactor and

analysis chamber through gate valves in ~60 sec using magnetically coupled translation devices (2). Samples could be heated resistively to 1600 K by attaching the plug to a four-lead electrical feedthrough in either chamber.

The reactor was operated at pressures up to 10 Torr by feeding cryogenically purified gases through stainless-steel lines and pumping through a mechanical pump ($P > 10^{-2}$ Torr) or a tubomolecular pump (10^{-3} to 10^{-8} Torr). The pumping time constant was adjusted between 0.25 and 10 sec to obtain measurable reactant conversions. Conversions were usually kept between 1 and 20% of the limiting reactant so that differential rates could be obtained. For high rates the conversion were sometimes as high as 50% and rates had to be corrected to values at the feed pressures.

Platinum foils were cleaned by heating in O_2 in the analysis chamber until only Pt AES peaks were observed. They were then transferred to the reactor where pressures and flow rates were adjusted. Rates were determined by measuring partial pressures with a differentially pumped quadrupole mass spectrometer using the mixed reactor equation

$$r_i = (VN_0/\tau ART_g)\,\Delta P_i \qquad (7)$$

where r_i and P_i are rate and partial pressure of species i, τ the residence time, A the catalyst surface area, N_0 Avogadro's number, V the volume of the reactor, and T_g the gas temperature (300 K). Rates in two reactant systems were typically reproducible to within ±10% on a given sample and are regarded as accurate to within at least ±50% for most conditions. Rates in CH_4, NH_3, O_2 mixtures were less accurate because of cracking fragment corrections.

After reaction, the reactor was evacuated and the sample was transferred into the analysis chamber where coverages were determined by AES and temperature-programmed desorption (TPD). No metal or gaseous contaminants with coverages above 0.05 monolayer were observed in any experiments reported here. Less than 0.5 monolayer of carbon (calibrated against a low-pressure CO monolayer) was produced by long exposures (1 Torr, 10^9 Langmuir) of either NH_3 at any temperature or CH_4 at 300 K (*3*). Exposure to O_2 at 1 Torr produced no detectable contaminants. Samples were cooled in reacting gases and then evacuated. Surface compositions could therefore change, although it is reasonable to assume that saturated surfaces remain essentially unchanged during cooling and pumpdown.

RESULTS

Rates in CH_4 + NH_3 + O_3

It is clearly impossible to examine the rates of individual reactions in the three component mixture with at least 15 simultaneous reactions, Eq. (6), but rates of production of species can be measured easily. Since HCN is produced near a 1 : 1 CH_4 : NH_3 ratio, this fuel ratio should be the most important and was the only one examined quantitatively.

Figure 1 shows a plot of rates versus partial pressure of O_2 up to 1 Torr for 1 Torr each of CH_4 and NH_3 at 1450 and at 1000 K. Rate measurements are based on the rate of production of the species indicated using Eq. (7). For CO and N_2 the parent molecules have identical masses, but they were distinguished by measuring mass 12 (C^+ from CO), and subtracting the calculated signal of CO from the total mass 28 to obtain each species.

Figure 1 shows that the rate of HCN production decreases with increasing P_{O_2} above P_{O_2} = 0.2 Torr. At higher P_{O_2} the N_2, CO and NO rates increase rapidly. The rate of HCN formation in the absence of O_2 is identical to rates reported previously (*3*). Nitric oxide is the dominant product above P_{O_2} = 0.5 Torr and is more significant at higher temperatures. CO_2 was always observed to have a low rate of production. Rates measured at 1200 K were intermediate between those shown here. All rates were reproduced on two foils, and all rates

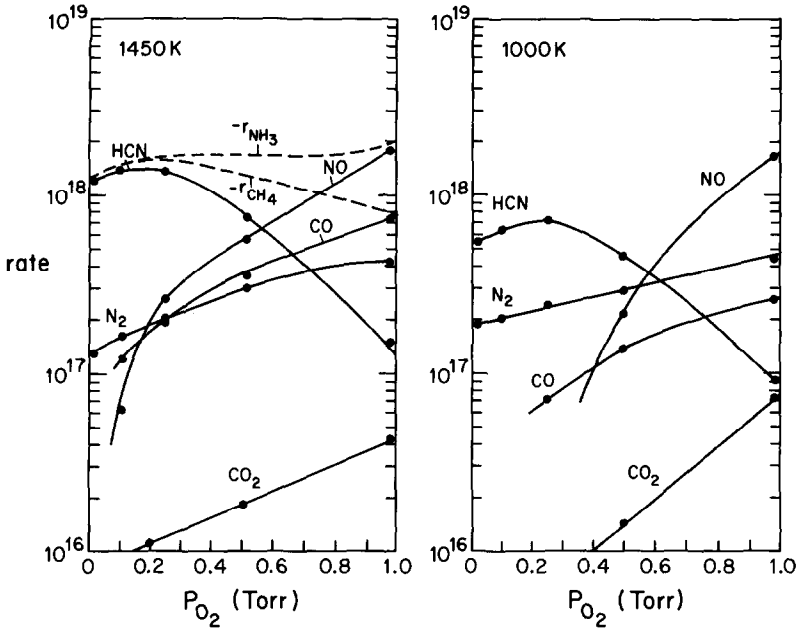

FIG. 1. Plot of rates of formation of species shown in molecules/cm² sec versus P_{O_2} for $P_{CH_4} = P_{NH_3}$ = 1 Torr at 1450 and at 1000 K. Without O_2, HCN is formed with ~90% selectivity, but addition of O_2 produces NO, CO, N_2, and CO_2 and a decrease in HCN. Nitric oxide is the major oxidation product, and addition of O_2 severely reduces HCN production.

are regarded as accurate to within at least a factor of 3. Rates are least accurate for CO_2 production which has the lowest rate.

Surface Analysis

After measuring rates at 1450 K, the sample was allowed to cool, the reactor was pumped down, and the sample was transferred into the analysis system for surface characterization by AES.

Figure 2 shows AES spectra for 1 : 1 : 1, 2 : 1 : 1, 1 : 2 : 1, and 1 : 1 : 2 mixtures of CH_4, NH_3, and O_2 for 1 or 2 Torr of each species. Comparable AES spectra of CH_4 and NH_3 alone were shown previously (*3*). The peak at ~380 eV is from both N and Pt. The nitrogen coverage was roughly proportional to the carbon coverage, and, using reasonable values of AES sensitivities (*3*), the C and N densities were nearly identical in the presence of O_2. Both N and C desorbed readily upon heating to 1100 K; this is therefore a "soft" form of carbon rather than graphite which must be oxidized off by heating in O_2. The probable form of C and N on these surfaces is the nitrile group, although multilayers of graphite form upon heating in pure CH_4 and a monolayer of N forms in pure NH_3.

Figure 3 shows a plot of the C_{270}/Pt_{237} AES peak–height ratio versus $P_{CH_4}/(P_{CH_4} + P_{NH_3})$, the upper curve is from CH_4 + NH_3 mixtures (*3*) and the lower with 1 Torr of O_2 present (data from Fig. 2). It is seen that the carbon coverage increases with increasing P_{CH_4} and that there is considerably less carbon in the presence of O_2. The coverage of of carbon, calibrated againt the saturation coverage of CO assuming C/Pt $\simeq$ 0.6 for one monolayer, is less than one monolayer in these experiments.

CH_4 Oxidation

In these experiments the formation of CO and CO_2 from mixtures of CH_4 and O_2 was studied for total pressures between 0.05 and 1.0 Torr for $CH_4 : O_2$ ratios between 1 : 4 and 4 : 1. A residence time of 0.25 sec

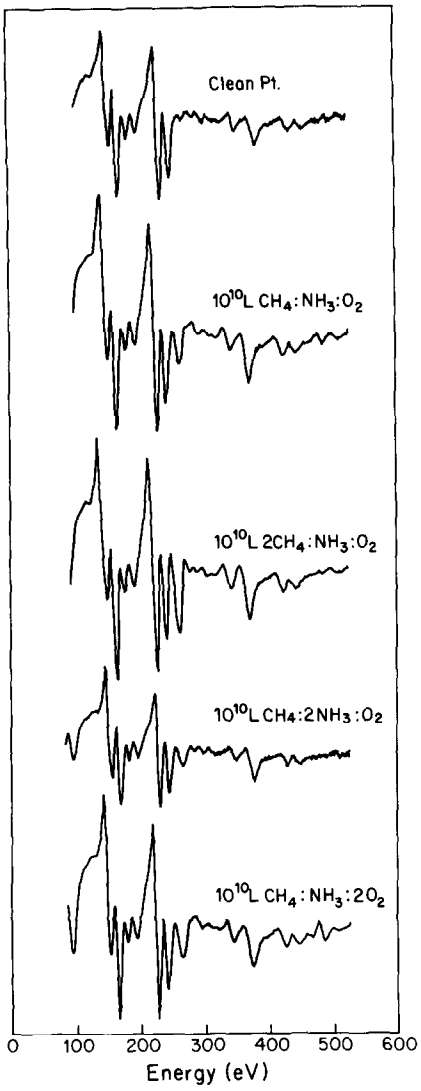

FIG. 2. AES spectra following 10^9 Langmuir (1 Torr for 1000 sec) exposures to CH_4, NH_3, O_2 mixtures at 1400 K for compositions indicated. No contamination is evident, and the only surface species are C, N, and O. Only in excess O_2 is surface oxygen detected. The C and N coverages increase as the CH_4/NH_3 ratio is increased, but in all cases the C and N coverages are less than one monolayer.

was used to maintain the conversion below 10% except for excess O_2 where the CH_4 conversion was as high as 20%.

Figures 4 and 5 show r_{CO} and r_{CO_2} vs T for $P_{O_2} = 0.25$ and 1.0 Torr, respectively. It is seen that $r_{CO} \gg r_{CO_2}$ except below ~900 K where they become comparable. The rate of CO production also increases monotonically while r_{CO_2} exhibits a maximum. Carbon monoxide oxidation on Pt (*11*, *12*) exhibits a sharp maximum and then decreases with increasing temperature as observed in Fig. 4.

In excess CH_4, r_{CO} becomes independent of temperature above 900 K, and the rate becomes zeroth order in CH_4. This observation indicates that the reaction becomes O_2^--flux limited in excess CH_4 above ~1000 K.

Figure 6 shows plots of r_{CO} versus P_{CH_4} and P_{O_2} for fixed partial pressures of the other reactant shown in the figure. The rate approaches zeroth order in both species in large excesses, and both rates approach a positive order in the limiting reactant. The slopes from Fig. 6 give a maximum slope of ~0.9 with respect to CH_4 from which we refer that the rate becomes first order in CH_4. The oxygen dependence is lower, ~0.7 which could indicate half or first order. For modeling we shall assume that the rate approaches half-order in O_2 in excess CH_4.

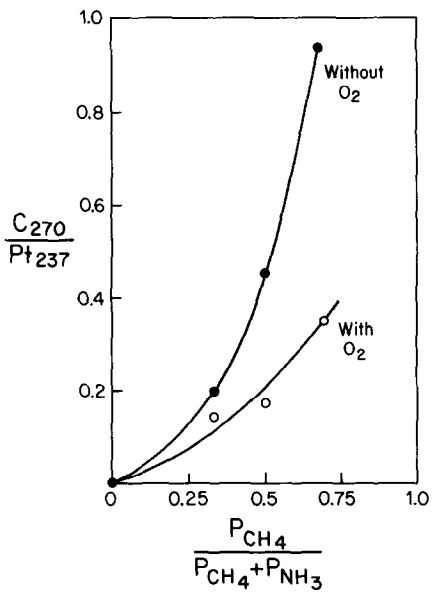

FIG. 3. Plot of AES C_{270}/Pt_{237} peak ratio versus fraction of CH_4 in CH_4–NH_3 mixtures. Without O_2 (*3*) the carbon coverage is much higher than with oxygen. Open circles are data from Fig. 2.

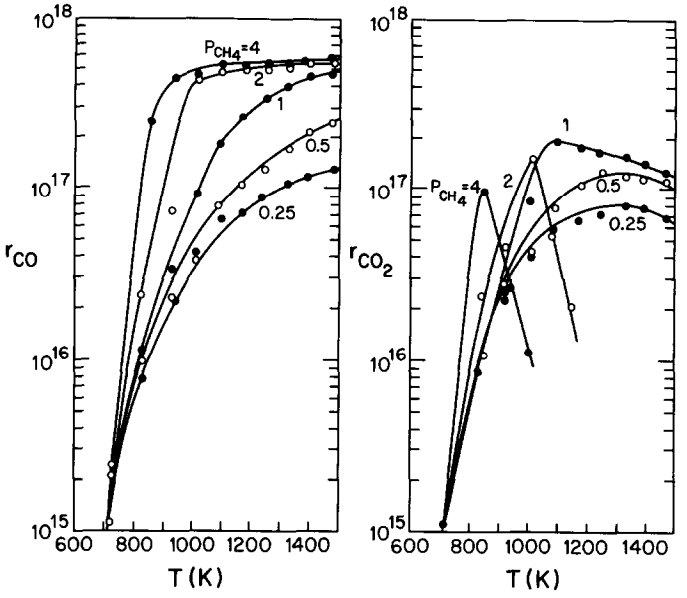

FIG. 4. Plot of r_{CO} and r_{CO_2} in the $CH_4 + O_2$ reactions versus Pt foil temperature for $P_{O_2} = 0.25$ Torr at CH_4 pressures indicated. r_{CO} increases monotonically and becomes O_2 flux limited for $P_{CH_4} \geq 2$ Torr. r_{CO_2} exhibits a sharp maximum in excess CH_4, and r_{CO_2} is always much less than r_{CO} except in large excess of O_2.

CH_4 + NO Reactions

The rates of HCN formation and NO consumption were measured in these experiments. Because both CO and N_2 are at mass 28, the rate of N_2 formation was obtained by subtracting the rate of HCN formation from NO consumption rather than attempting to monitor N_2 directly.

Rates were measured for CH_4 pressures

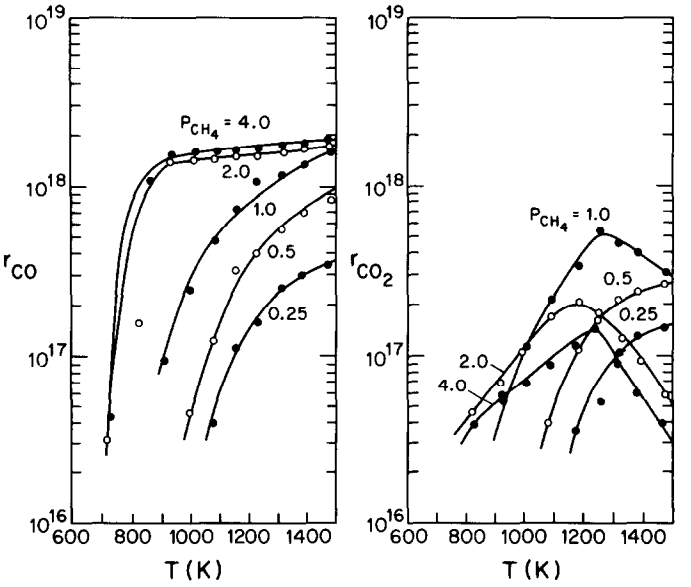

FIG. 5. Plot of r_{CO} and r_{CO_2} in the $CH_4 + O_2$ reactions versus Pt foil temperature for $P_{O_2} = 1.0$ Torr for CH_4 pressures indicated. Behavior is qualitatively similar to Fig. 4 except that the maximum in r_{CO_2} is shifted to higher temperatures at higher P_{O_2}.

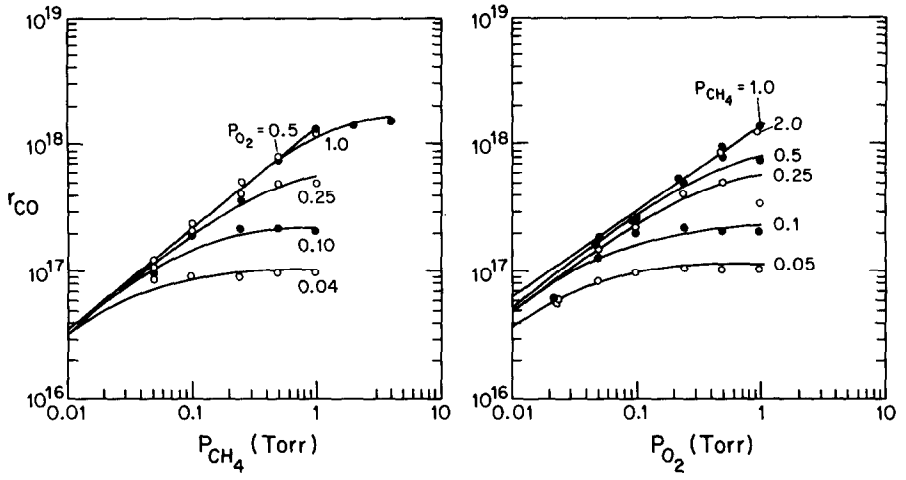

FIG. 6. Plot of r_{CO} at 1450 K versus P_{CH_4} and P_{O_2} at pressures indicated for the other species. Rates are first order in P_{CH_4} and half-order in P_{O_2} at low pressures and approach zeroth order at high pressures of each species.

between 0 and 4.0 Torr and NO pressures between 0.10 and 4.0 Torr. Figures 7 and 8 show r_{HCN} and r_{N_2} versus temperature for P_{NO} = 0.25 and 1.0 Torr, respectively. It is seen that r_{HCN} increases monotonically whereas r_{N_2} exhibits a maximum at low temperature (900 K) and then a minimum at ~1100 K.

Figure 9 shows plots of r_{HCN} and r_{N_2} versus P_{CH_4} at 1450 K for values of P_{NO} in the figure. It is seen that the order of r_{HCN} in P_{CH_4} is between 0.5 and 0.7. We shall assume that r_{HCN} is first order in P_{CH_4} for low P_{CH_4} and becomes zeroth order in methane at high P_{CH_4}. Examination of Fig. 9 also shows that r_{HCN} is nearly first order in P_{NO} at all P_{NO}.

The nitrogen production rate r_{N_2} appears

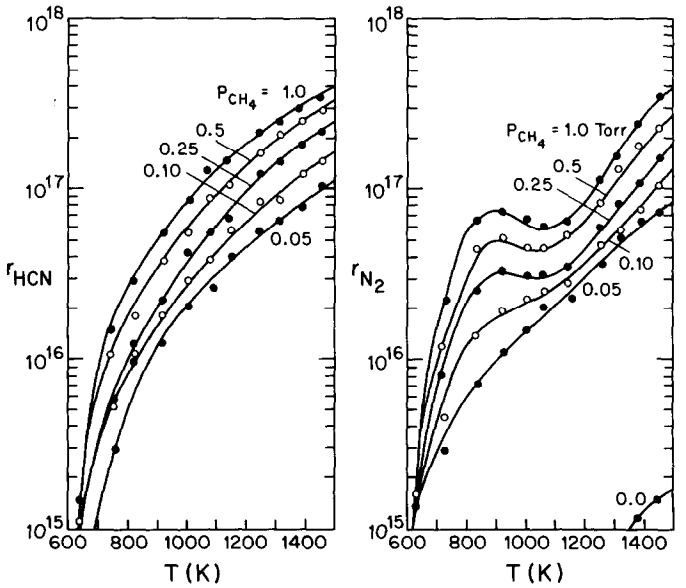

FIG. 7. Plot of r_{HCN} and r_{N_2} in the CH_4 + NO reaction versus surface temperature on polycrystalline Pt at P_{NO} = 0.25 Torr. r_{HCN} increases monotonically with surface temperature, while r_{N_2} exhibits a maximum and a minimum.

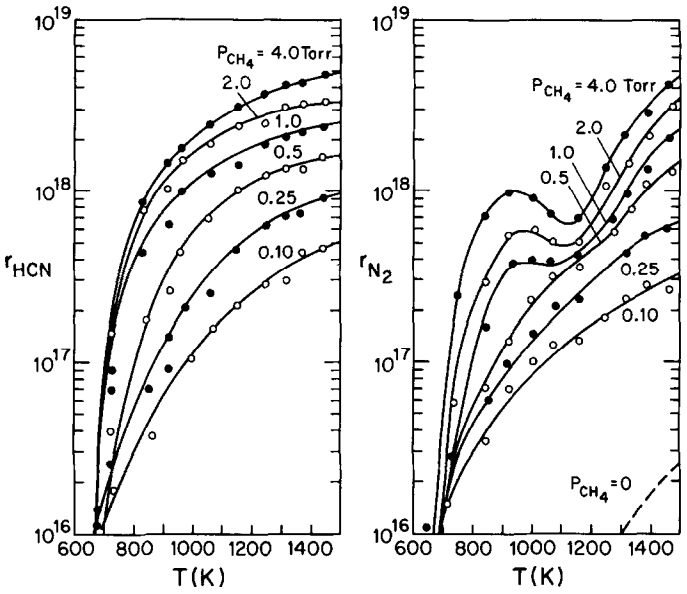

FIG. 8. Plot of r_{HCN} and r_{N_2} in the CH_4 + NO reaction versus surface temperature on polycrystalline Pt at P_{NO} = 1.0 Torr. Rates are qualitatively similar to those in Fig. 7.

to change from approximately first order in P_{CH_4} to less than one-third order as P_{NO} decreases from 1.0 to 0.1 Torr. The existence of a maximum and a minimum in r_{N_2} shows that the kinetics of this reaction must be more complex than could be described through a single LH rate expression.

When P_{CH_4} = 0 the N_2 production rate is more than an order of magnitude lower than when P_{CH_4} = 0.1 Torr as shown by the curve in the lower right corner of Fig. 8. This difference is strong evidence that CH_4 enhances NO decomposition and that the reactions in Figs. 7 and 8 are in fact bimolecular.

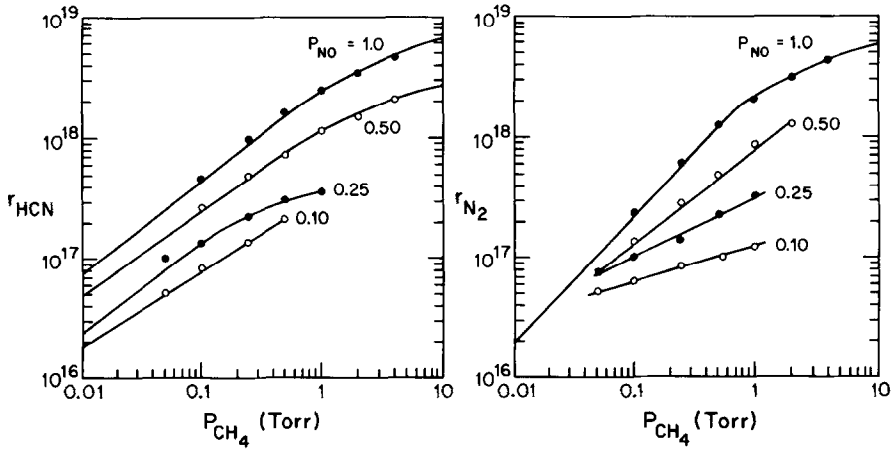

FIG. 9. Plot of r_{HCN} and r_{N_2} in the CH_4 + NO reactions versus P_{CH_4} at 1450 K. r_{HCN} is approximately 0.7 order in CH_4 and is first order in NO. r_{N_2} goes from first order in CH_4 to a small order as P_{NO} decreases.

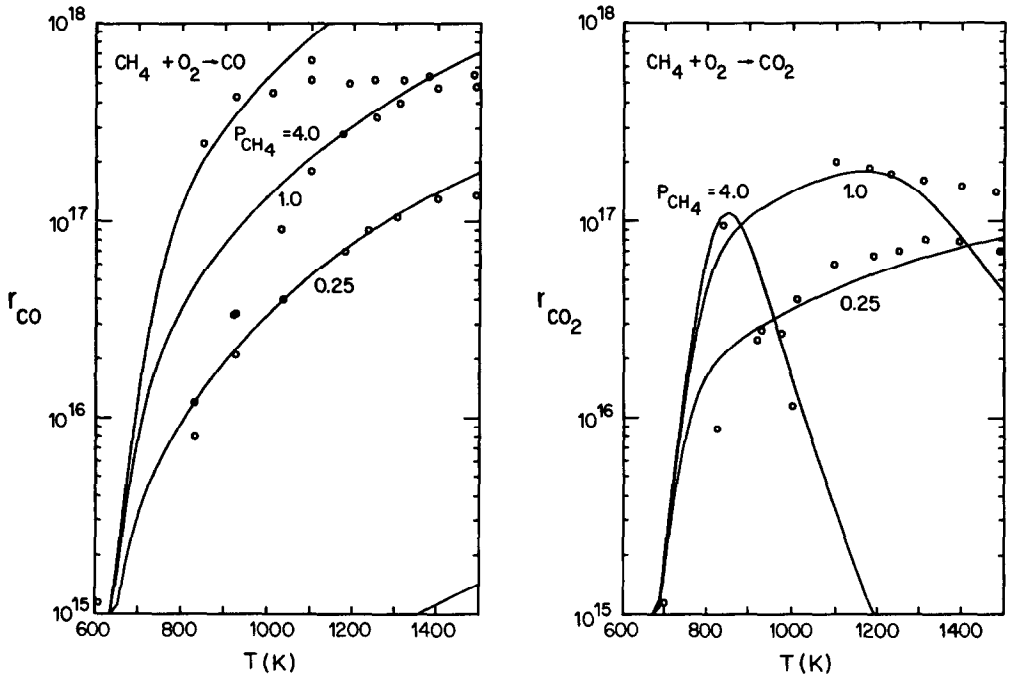

FIG. 10. Calculated rates of CO and CO_2 production in the $CH_4 + O_2$ reaction compared to rate data from Fig. 5. Curves shown are from Eqs. (9) and (12), respectively.

DISCUSSION

CH_4 Oxidation

Methane oxidation by O_2 to CO has a much higher rate than to CO_2 for all compositions and temperatures in these experiments. We shall attempt to formulate rate expressions which fit the observed rates and discuss the mechanisms consistent with them.

At high temperature CO formation is nearly first order in CH_4 and half-order in O_2, while at low temperature the rate is approximately zeroth order in CH_4 and remains half order in O_2 (Fig. 5). This suggests a rate expression of the form

$$r_{CO} = \frac{k_R K_{CH_4} K_{O_2}^{1/2} P_{CH_4} P_{O_2}^{1/2}}{1 + K_{CH_4} P_{CH_4}} \qquad (8)$$

which is predicted in an LH model if CH_4 and O_2 are noncompetitively adsorbed with O_2 dissociated. In this expression K_{CH_4} and K_{O_2} are adsorption equilibrium constants and k_R is the surface reaction rate coefficient. The data of Figs. 4 and 5 were fit to these expressions assuming Arrhenius temperature dependences for K's and k_R. Figure 10 shows calculated rate curves for $P_{O_2} = 0.25$ Torr for P_{CH_4} values indicated with data from Fig. 4. Curves agree with all data points within approximately a factor of 3 except at $P_{CH_4} = 4$ where the rate becomes temperature independent. The rate expression used in Fig. 10a was

$$r_{CO} = \frac{4 \times 10^{19} \exp[-10{,}000/RT] P_{CH_4} P_{O_2}^{1/2}}{1 + 5 \times 10^{-10} \exp[+30{,}000/RT] P_{CH_4}} \qquad (9)$$

with r_{CO} in molecules/cm^2 sec, pressures in Torr, and activation energies in cal/mole. This model predicts a 30 kcal/mole heat of adsorption for whatever species forms from CH_4 to block reaction at high P_{CH_4} and low temperatures. k_{CO} and K_{O_2} are not obtainable independently from this expression because the numerator is a product of these quantities, Eq. (8).

In excess CH_4, r_{CO} becomes independent

of T and of P_{CH_4} and is evidently O_2 flux limited. Maximum rates of Figs. 4 and 5 are 5×10^{17} and 2×10^{18} at $P_{CH_4} = 0.25$ and 1.0 Torr, espectively. Since the flux of O_2 is calculated to be 1×10^{21} and 2.5×10^{20} at these O_2 partial pressures (ideal gas at 300 K), these results give

$$r_{CO} = 5 \times 10^{18} P_{O_2} \tag{10}$$

in the O_2 mass transfer limit with the reaction probability of O_2 being 0.005.

Methane oxidation to CO_2 is much slower and exhibits a sharp temperature maximum in excess CH_4. This suggests a rate expression of the form

$$r_{CO_2} = \frac{K_1 P_{CH_4} P_{O_2}}{(1 + K_2 P_{CH_4})(1 + K_3 (P_{CH_4}/P_{O_2})^n)} \tag{11}$$

where K_1, K_2, and K_3 are groupings of constants. The first term in the denominator is from CH_4 saturation at low temperature, while the term containing $(P_{CH_4}/P_{O_2})^n$ can be obtained assuming graphite buildup in which carbon blocks n sites for O_2 adsorption. A similar model was developed for CH_4 inhibition of the $CH_4 + NH_3$ reactions (*2, 3*).

Figure 10b shows r_{CO_2} calculated from an expression of this form using the parameters

$$r_{CO_2} = \frac{7 \times 10^{18} \exp[-5000/RT] P_{CH_4} P_{O_2}}{(1 + 1 \times 10^{-11} \exp[+40{,}000/RT] P_{CH_4})(1 + 10^3 \exp[-40{,}000/RT](P_{CH_4}/P_{O_2})^6)} \tag{12}$$

The negative exponential in the second denominator term represents an activated carbon buildup which is larger at high temperatures and causes the rapid decrease in rate with increasing temperature in excess CH_4.

CH_4 + NO Reactions

Reaction to HCN predominates over reaction to N_2 except at low temperatures (<800 K) where rates appear to be comparable. We modeled HCN formation using an expression of the form

$$r_{HCN} = \frac{k_R K_{CH_4} K_{NO} P_{CH_4} P_{NO}}{1 + K_{CH_4} P_{CH_4}} \tag{13}$$

because the rate goes from zeroth to nearly first order in P_{CH_4} and is always approximately first order in P_{NO}. Figure 11 shows a fit of data from Fig. 8 with a rate expression

$$r_{HCN} = \frac{1.8 \times 10^{20} \exp[-10{,}000/RT] P_{CH_4} P_{NO}}{1 + 5 \times 10^{-10} \exp[30{,}000/RT] P_{CH_4}} \tag{14}$$

Again agreement is generally quite good except at high P_{CH_4} where the experimental rate falls below the calculated curves.

No temperature independent rate regime characteristic of an NO flux limit was observed, although the flattening of the upper curve of Fig. 10a may indicate the approach to a flux limit. The reaction probability of NO is calculated to be ~0.01 Fig. 8.

HCN formation does not exhibit CH_4 inhibition in excess CH_4 as did the $CH_4 + NH_3$ reaction (*3*). Evidently the presence of NO prevents a buildup of a reaction inhibiting species as it does in NH_3.

Also note that the CH_4 + NO reaction is slightly faster than the $CH_4 + O_2$ reaction. NO is thus a slightly better oxidizing agent than O_2, presumably because the sticking coefficient of NO is higher than that of O_2.

The CH_4 inhibition terms and the numerator activation energies in Eqs. (9) and (14) are identical. This suggests that low temperature inhibition of both reactions by CH_4 occurs by the *same species and processes* with both oxidizing agents.

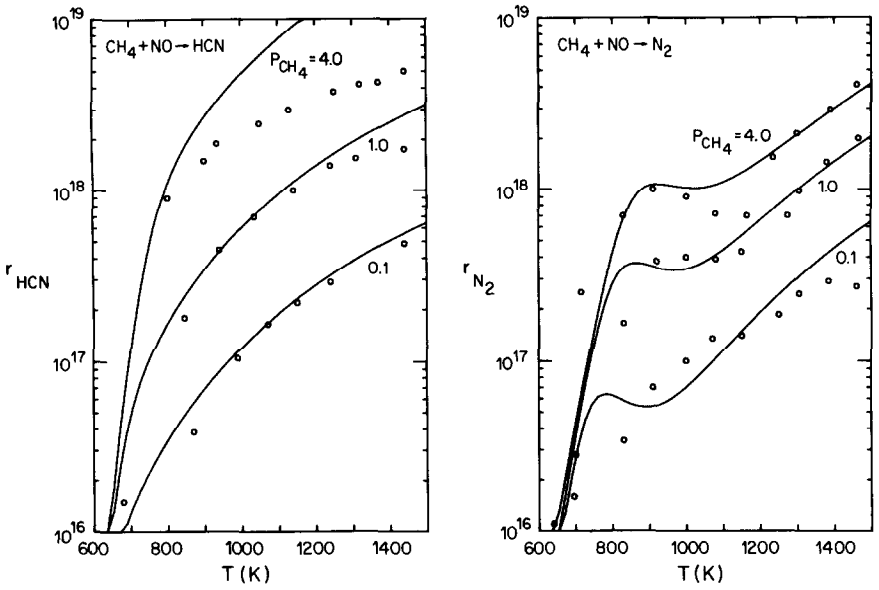

FIG. 11. Calculated rates of HCN and N_2 production in the CH_4 + NO reaction compared to data from Fig. 8. Curves shown are from Eqs. (14) and (16), respectively.

The rate of N_2 formation exhibits a maximum and a minimum as seen in Figs. 7 and 8. This would be difficult to fit in a single LH mechanism, and it suggests two processes. We assume a rate expression of the form

$$r_{N_2} = \frac{K_1 P_{CH_4} P_{NO}}{1 + K_2 P_{CH_4}} + K_3 P_{CH_4}^{1/2} P_{NO} \quad (15)$$

The pressure dependences shown fit the results well, but we do not suggest that they have any special significance.

Figure 11b shows a plot of data from Fig. 8 along with calculated curves for a rate expression

$$r_{N_2} = \frac{1.2 \times 10^{15} \exp[+10{,}000/RT] P_{CH_4} P_{NO}}{1 + 1 \times 10^{-11} \exp[40{,}000/RT] P_{CH_4}} + 3 \times 10^{20} \exp[-15{,}000/RT] P_{CH_4}^{1/2} P_{NO} \quad (16)$$

The first term dominates at low temperature and gives the rate maximum because of the negative activation energy in the numerator, while the second term dominates at high temperature because of its large positive activation energy.

Bimolecular Reaction Rates

Of the 15 reactions in the CH_4 + NH_3 + O_2 system (Eqs. (6.1)–(6.15)), all but HCN hydrolysis have been studied on Pt, and in rate expressions have been determined for most reactions. Table 1 lists rates calculated at 700, 1000, and 1400 K for each of these reactions for reactant pressures of 1 Torr along with references in which rates were obtained.

At 1400 K with 1 Torr of each reactant most rates are between 1×10^{17} and 3×10^{18} molecules/cm^2 sec. At this pressure only CH_4 + O_2 and H_2 + O_2 become flux limited. The reactant fluxes to the surface are $\sim 10^{21}$ molecules/cm^2 sec at 1 Torr so the calculated reaction probabilities at 1 Torr are 3×10^{-3} to 10^{-4}. Of course, all bimolecular reactions must become flux limited at sufficiently high pressures because the rate cannot exceed the flux of either reactant. Since conversions were kept low for data in Fig. 1, all reaction rates involving intermediates (NO, H_2, CO, CO_2, HCN) as reactants should be negligible in rates shown in Fig. 1.

TABLE 1

Bimolecular Reaction Rates in $CH_4 + NH_3 + O_2$ at Reactant Pressures of 1 Torr

Reaction	700 K	1000 K	1400 K	Reference
$CH_4 + NH_3 \rightarrow HCN$	8×10^{16}	2×10^{17}	5×10^{17}	*3*
$\rightarrow N_2$	1×10^{17}	1.8×10^{17}	1×10^{17}	*3*
$NH_3 + O_2 \rightarrow NO$	$\sim 1 \times 10^{17}$	$\sim 1 \times 10^{18}$	$\sim 3 \times 10^{18}$	
$\rightarrow N_2$	$\sim 2 \times 10^{18}$	$\sim 4 \times 10^{18}$	$\sim 6 \times 10^{17}$	*4*
$CH_4 + O_2 \rightarrow CO$	2×10^{16}	2×10^{17}	1×10^{18}	This work
$CH_4 + NO \rightarrow N_2$	1×10^{16}	8×10^{17}	3×10^{18}	This work
$NH_3 + NO \rightarrow N_2$	4×10^{17}	2×10^{18}	1×10^{18}	*10*
$CO + O_2 \rightarrow CO_2$	2×10^{17}	3×10^{18}	2×10^{18}	*11*
$H_2 + O_2 \rightarrow H_2O$	—	8×10^{17}	8×10^{17}	*14*
$CO + H_2O \rightarrow CO_2 + H_2$	1×10^{15}	4×10^{15}	7×10^{16}	*14*
$NO + CO \rightarrow N_2 + CO_2$	3×10^{17}	6×10^{18}	3×10^{18}	*15*

The Three Component Reactions

It is clearly not possible to model the $CH_3 + NH_3 + O_2$ reaction system in detail because (1) there are many stoichiometric reactions, Eq. (6), which can produce each product, (2) the accuracy of rate data for the multiple reactant system with many components does not justify detailed fits of any proposed model forms, and (3) there is a question as to the significance of decoupling multiple surface reactions.

For homogeneous reactions among three reactants, one would model the process as a sequence of unimolecular and bimolecular elementary reactions between reactants and reaction products. This is not necessarily valid for surface reactions because it is difficult to identify the elementary reaction steps.

Decoupling of reactions would be possible if coverages were sufficiently low that adsorbed species did not inhibit or promote reactions of other species and if reactivities were sufficiently low that a reaction of a particular species were uncoupled from its other possible reactions. For example, NH_3 forms HCN, N_2, and NO nitrogen products while CH_4 forms HCN, CO, and CO_2 carbon products. If one writes the total rate of CH_4 and NH_3 consumption

$$-r_{CH_4} = r_{HCN} + r_{CO} + r_{CO_2} \qquad (17)$$

and

$$-r_{NH_3} = r_{HCN} + 2r_{N_2} + r_{NO} \qquad (18)$$

one finds nearly constant rates of NH_3 and CH_4 consumption with total CH_4 and NH_3 reaction probabilities of approximately 0.01 at all P_{O_2} as shown in Fig. 1. Therefore the $CH_4 + NH_3 + O_2$ system should be regarded as a tightly coupled reaction system in which O_2 only changes the selectivity but not the total reactivity of CH_4 and NH_3.

In fact, the selectivity of products formed in $CH_4 + NH_3 + O_2$ agrees very well with relative rates and with rate expressions of the unimolecular and bimolecular reactions of Eq. (6). These expressions predict that NH_3 oxidation is favored over CH_4 oxidation and that CO formation should be favored over CO_2 as observed. When we assumed that rates were decoupled and wrote rates as Eq. (6) using the six major unimolecular and bimolecular rate expressions(*13*), we obtained good agreement with Fig. 1.

The experiment of Fig. 1 was in a mixed reactor at low residence time and low conversion. This reduces the effect of series reactions of intermediates and products so that NO and CO are major products with little reaction on to N_2 and CO_2. We shall discuss modeling of the three compoent system at higher pressures and in a high conversion reactor in a later publication.

It is instructive to consider the $CH_4 +$

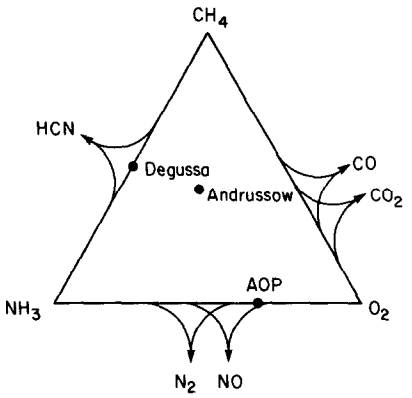

FIG. 12. Sketch of feed compositions and products formed in the $CH_4 + NH_3 + O_2$ reactions. Assumptions of bimolecular reactions yields products shown at stoichiometrics indicated on each leg of the diagram. Feed compositions used in the industrial reactions of these species are shown as points in the diagram.

$NH_3 + O_2$ system on a triangular diagram as shown in Fig. 11. If products were formed by bimolecular steps, each side of the triangle produces the products indicated, ignoring H_2 and H_2O which are additional products of all reactions. The industrial HCN processes (Degussa and Andrussow) and the NH_3 oxidation process (AOP) use initial feed compositions indicated by the point on the diagram, and the selectivities to HCN and NO respectively determine reactor performance.

SUMMARY

The major reaction yielding HCN in CH_4, NH_3, O_2 mixtures appears to be the $CH_4 + NH_3$ reaction. Oxygen reacts with NH_3 to form NO faster than with CH_4 to form CO, although in a reactor at high conversions NO may react with CH_4 to form HCN.

The bimolecular reactions $CH_4 + O_2 \rightarrow$ CO and $CH_4 + NO \rightarrow$ HCN are very fast and have essentially identical rate expressions with the NO reaction being faster by a factor of ~3 at all temperatures. Both can be fit quite accurately by Langmuir–Hinshelwood rate expressions to within the accuracy of the rate data. No inhibition of either oxidation reaction by excess CH_4 is evident, although the complete oxidation reactions to form CO_2 and N_2 respectively are strongly inhibited in excess CH_4.

In a later paper we shall discuss modeling of the Andrussow and ammonia oxidation reactors using rate parameters from individual bimolecular reactions. In high pressure situations the coupling between reactions and flux limited rates may have a significant influence on observed products.

REFERENCES

1. Satterfield, C. N., "Heterogeneous Catalysis in Practice," p. 221. McGraw–Hill, New York, 1980.
2. Hasenberg, D., and Schmidt, L. D., *J. Catal.* **91,** 116 (1985).
3. Hasenberg, D., and Schmidt, L. D., *J. Catal.* **97,** 156 (1986).
4. Pignet, T. P., and Schmidt, L. D., *J. Catal.* **40,** 212 (1975).
5. Gland, J. L., and Korshak, V. N., *J. Catal.* **53,** 9 (1978); **61,** 543 (1980).
6. Dixon, J. K., and Longfield, J. E., *Catalysis* **7,** 1123 (1979).
7. Trimm, D. L., and Lam, C. W., *Chem. Eng. Sci.* **35,** 1405 (1980).
8. Lintz, H. G., Pentenero, A., and le Goff, P. L., *J. Chim. Phys.* **59,** 933 (1962); *in* "Second European Conference on Surface Physics, Enshede, Netherlands," 1972.
9. Firth, J. G., and Holland, H. B., *Trans. Faraday Soc.* **65,** 1121 (1969).
10. Takoudis, C. G., and Schmidt, L. D., *J. Catal.* **80,** 274 (1983).
11. Engel, T., and Ertl, G., *Adv. Catal.* **28,** 1 (1979).
12. Hori, G. K., and Schmidt, L. D., *J. Catal.* **38,** 335 (1975).
13. Hasenberg, D., Ph.D. thesis, University of Minnesota, 1985.
14. Bleiszner, J., Ph.D. thesis, University of Minnesota, 1979.
15. Klein, R. L., Schwartz, S. B., and Schmidt, L. D., *J. Phys. Chem.* **89,** 4908 (1985).